BOND GRAPH MODEL CONDITIONING FOR ANALYSIS, SIMULATION AND CONTROL SYSTEM DESIGN: *APPLICATION TO A PLANAR MOBILE ROBOTIC MANIPULATOR*

Matías Nacusse[a,b], Martín Crespo [a,b], Sergio Junco [a], Vitalram Rayankula[c], Pushparaj Mani Pathak[c]

[a] Laboratorio de Automatización y Control (LAC), Departamento de Control, FCEIA, UNR. Rosario, Argentina
[b] CONICET: Consejo Nacional de Investigaciones Científicas y Técnicas. Argentina
[c] Department of Mechanical and Industrial Engineering, Indian Institute of Technology Roorkee, India

[a] {nacusse, crespom, sjunco}@fceia.unr.edu.ar
[c] rvitalram@gmail.com, pushpfme@iitr.ac.in

ABSTRACT

The appearance of algebraic constraints among energy variables in models of physical systems leads to sets of (possibly nonlinear) implicit state equations, which usually complicate the treatment of the problems to be solved on the model. Building up on the Bond Graph model of a Planar Mobile Robotic Manipulator, this paper discusses some techniques to handle this kind of situations, determined here by the coupling of rigid bodies. Two alternatives to break the constraints are presented, consisting in the insertion between the coupled elements of: a) parasitic components –mostly spring-dampers, which is standard practice– or b) residual sinks – which is equivalent to the practice of adding constraint forces. Modifying the Bond Graph through the introduction of storage fields is the third method presented. Further, the extraction of constraint-free Euler-Lagrange and Hamiltonian descriptions from the Bond Graph are addressed. Finally, the suitability of all of these five alternatives for the purposes of simulation, analysis and control system design are discussed, and illustrated with simulation results.

Keywords: Planar mobile manipulator, Bond Graphs, Euler-Lagrange equations, Port-Hamiltonian systems, Simulation, Nonlinear control.

1. INTRODUCTION

The multidomain nature of modern engineering systems has renewed the interest in energy-based modeling formalisms. This is above all true in Mechatronics in general and Robotics in particular. Euler-Lagrange (EL) modeling is the classical approach in Robotics (Siciliano et al., 2009). Since relatively recent times the Hamiltonian formalism under the new, extended Port-Hamiltonian System (PHS) version has also been considered for the purposes of nonlinear control system synthesis, mainly in the framework of Passivity-Based Control (PBC) (Ortega et al., 2002). Besides these two modeling approaches rooted in Classical Physics, the Bond Graph (BG) technique, an engineering graphical modeling method, has gained importance (Karnopp, Margolis and Rosenberg, 2006), (Merzouki et al., 2012). It uses a reduced and unified set of symbols –which describe basic energy phenomena and interconnection structure in a physical system– able to represent not only the mechanical parts of a multidomain system, but also the electromechanical actuators and their associated power electronic converters, pneumatic or hydraulic actuators, etc.

One of the advantages of BGs is their modular or object-oriented modeling nature which allows to construct the whole system model by coupling the models of its subsystems. However, this advantage comes with a drawback in certain cases: when the system order is lower than the number of energy variables, there appear algebraic constraints among them, fact that leads to sets of implicit state equations (Karnopp, Margolis and Rosenberg, 2006). Graphically, this translates into storages being in *derivative causality* and the presence of algebraic loops or zero order causal paths (ZCP), see (van Dijk and Breedveld, 1991) for a classification. This is a recurrent problem when modeling mechanical systems, especially in systems with kinematic constraints. The existence of ZCP always implies that the set of state equations is an implicit set of Differential-Algebraic Equations (DAEs) with the consequent problems to the numerical solvers, see for example (van Dijk and Breedveld, 1991) or (Cacho, Felez and Vera, 2000) for the numerical issues in solving these systems. Modern modeling and simulation (M&S) software is equipped with tools capable to handle implicit systems, but they frequently fail when the algebraic dependence is complex. In these cases, while still useful for direct analysis of some system properties, the BG models are not immediately useful for simulation or control system design. They must be suitably adapted for those purposes. To deal with ZCPs the authors in (Karnopp and Margolis, 1979) add some parasitic components to break the causal loops. While this classic engineering approach is simple to implement, it is not always evident how to parameterize the parasitic components, and results in highly stiff models of higher order which increase the total simulation time and, occasionally, the numerical errors too. An alternative technique to break the ZCPs without modifying the dynamics consists in adding residual sinks (rS) in adequate positions of the causal paths (Gawthrop and Smith, 1992) (Borutzky and Cellier, 1996). This resource has been incorporated in certain simulation tools via programming commands, called "*constraint*" in some of them (20sim®, for instance, see (Controllab Products, n.d.)). This method solves the problem calculating efforts that enforce the geometric or kinematic constraints producing the ZCP. As it proceeds numerically at each simulation step, it could increase the total simulation time and accumulate errors beyond admissible limits. This problem can be circumvented when the constraint can be explicitly solved and embodied in the residual sink (Nacusse and Junco, 2017), as it is done in the example case treated in this paper. A radical different approach is to collect the dependent storage phenomena in a so called *storage field* (Karnopp, 1992). This approach, while abandoning the modular feature of the BGs, yields a model without ZCPs between energy storage elements. Another solution, which is directly in line with the construction of the storage field, consists in choosing sets of independent coordinates in the BG model and to derive EL- or PHS-models from it (Karnopp, 1977) (Donaire and Junco, 2009) (van der Schaft and Jeltsema, 2014).

The main goal of this paper is to present the derivation and discuss the application of the full panoply of the previously mentioned alternative models starting from a BG of a planar mobile robotic manipulator (PMRM) featuring derivative causality. Even if issues related to analysis and control synthesis and design are considered, the main stress is put on simulation matters.

The rest of the paper is organized as follows. Section 2 briefly reviews the EL and PHS formalisms and describes the PMRM. The construction of the BGs is done in Section 3. First the base BG in derivative causality is built and then it is shown how to get the models with rS or parasitic elements to break the ZCPs. Second, following the procedure detailed in (Karnopp, 1992), a BG featuring an *IC-Field* is derived as a means to avoid the derivative causality. Section 4 compactly discusses the derivation of EL and PHS models from the BGs previously introduced. Section 5 presents some simulation results with the PMRM in closed-loop to compare the differents approaches in terms of simulation time and error. Finally, some conclusions are given in Section 6.

2. MODELING FORMALISMS AND SYSTEM DESCRIPTION

2.1. Modeling formalisms

The EL equations are probably the most classical approach to modeling in the field of robot dynamics. These equations are obtained performing the operations indicated in (1) on the Lagrangian function $\mathcal{L}(q,\dot{q}) = \mathcal{T}^*(\dot{q}) - \mathcal{V}(q)$, where $\mathcal{T}^*(\dot{q})$ is the kinetic co-energy, $\mathcal{V}(q)$ is the potential energy, q and $\dot{q}$ are the vector of generalized coordinates and velocities respectively, and E is the vector of generalized non-conservative forces.

$$\frac{\mathrm{d}}{\mathrm{dt}}\left(\frac{\partial\mathcal{L}}{\partial\dot{\mathrm{q}}}\right) - \frac{\partial\mathcal{L}}{\partial\mathrm{q}} = \mathrm{E} \tag{1}$$

Since more recently, a Hamiltonian formulation of the system dynamics called PHS has gained importance in robotics because of the benefits it offers through the application of the Passivity-Based Control (PBC) techniques to robot control problems (Ortega et al., 2001). Classically, the Hamilton equations of motion are derived from (1) via the definition of the generalized momenta $p := \partial\mathcal{L}/\partial\dot{q}$ and the Legendre transformation $\mathfrak{G}\{\mathcal{L}(q,\dot{q})\} := p^T\dot{q} - \mathcal{L}(q,\dot{q})$. This yields the Hamiltonian state function as $\mathcal{H}(q,p) = \mathfrak{G}\{\mathcal{L}(q,\dot{q})\} = T(p,q) + V(q)$, where $T(p,q)$ is the kinetic energy in the system. Furthermore, operating on (1), and assuming a system with n degrees of freedom, the following Hamiltonian model is obtained:

$$\underbrace{\begin{bmatrix}\dot{\mathrm{q}}\\ \dot{\mathrm{p}}\end{bmatrix}}_{\dot{\mathrm{x}}} = \underbrace{\begin{bmatrix}0_{\mathrm{nxn}} & \mathrm{I}_{\mathrm{nxn}}\\ -\mathrm{I}_{\mathrm{nxn}} & 0_{\mathrm{nxn}}\end{bmatrix}}_{\mathrm{J}} \underbrace{\begin{bmatrix}\frac{\partial\mathcal{H}(\mathrm{x})}{\partial\mathrm{q}}\\ \frac{\partial\mathcal{H}(\mathrm{x})}{\partial\mathrm{p}}\end{bmatrix}}_{\nabla_{\mathrm{x}}\mathcal{H}(\mathrm{x})} + \begin{bmatrix}0_{\mathrm{n}}\\ \mathrm{E}\end{bmatrix} \tag{2}$$

This classical model is a particular case of the PHS form (3), which explicitly shows the presence of dissipation in the system, and admits state variables other than q and p describing the system dynamics (van der Schaft and Jeltsema, 2014).

$$\dot{x} = [J(x,u) - R(x,u)]\,\nabla_x\mathcal{H} + g(x)\,u \tag{3}$$

Here $J(x,u)$ is the structure or interconnection matrix which conserves the skew-symmetric property of J in the classical formulation, but does not need to be composed by unitary submatrices. The dissipation matrix $R(x,u)$ is a symmetric, positive (semi–) definite matrix, and $g(x)$ is a matrix weighting the inputs u. This latter vector is composed of control and, possibly, disturbance inputs. The presence of x and u as arguments of J and R takes into account the fact that some interconnection or dissipation elements could be state-dependent (the magnetic flux modulating the electromechanical power exchange in an electric actuator, for instance) in the case of x, and that control actions u could be exerted through the interconnection structure (as in power electronic converters feeding electromechanical actuators) or the dissipation structure (as in a hydraulic control valve).

In this paper the BG approach, an energy-based graphical modeling formalism (Karnopp, Margolis and Rosenberg, 2006), is resorted to as the primary modeling tool. Indeed, starting from a first BG model, other BGs are derived aiming at different purposes, as well as an EL and a PHS model of the PMRM under consideration.

2.2. System description

The physical system, shown in Figure 1, is a PMRM consisting of a mobile base (MB) coupled to a manipulator arm (MA) with two rigid links connected by revolute joints. The MB is a circular platform driven by

three independent Omniwheels symmetrically located at 120 degrees each other.
The following set of fourteen relevant coordinates can be distinguished in the sketch of Figure 1:

$$\{\Omega_{w1},\Omega_{w2},\Omega_{w3},x_0,y_0,\phi_0,\phi_1,\phi_2,x_1,y_1,x_2,y_2,\theta_1,\theta_2\} \quad (4)$$

where: $\Omega_{w1,2,3}$ are the rotational angular positions of the three wheels; $x_{0,1,2}$ and $y_{0,1,2}$ are the positions of the centers of mass (CoM) of the MB and the two links with respect to the inertial Cartesian frame (X_F,Y_F); $\phi_{0,1,2}$ specify, respectively, the angular positions of the attachment point of link 1 to the MB and of links 1 and 2, all the three of them measured with respect to the X_F axis; and $\theta_{1,2}$ are the relative angular positions of the links, as indicated in Figure 1. This is not a set of independent coordinates. As the three wheels are independently actuated, a restriction between the subsets $\{\dot{\Omega}_{w1},\dot{\Omega}_{w2},\dot{\Omega}_{w3}\}$ and $\{\dot{x}_0,\dot{y}_0,\dot{\phi}_0\}$ can be derived, which can be expressed by an invertible matrix, as done in the next section. Under the assumption of holonomy of the MB, this relationship enforces a restriction among the respective coordinates. Also the subsets $\{\theta_1,\theta_2\}$ and $\{\phi_1,\phi_2\}$ are each other dependent. Finally, as shown in equation (5), $x_{1,2}$ and $y_{1,2}$ can be written in terms of $x_0,y_0,\phi_0,\phi_1,\phi_2$. As usual in Robotics, the short notations $s_\phi = \sin(\phi)$ and $c_{\phi_1} = \cos(\phi)$ have been used.

$$\begin{aligned}
x_1 &= x_0 + l_b c_{\phi_0} + l_1 c_{\phi_1}\\
y_1 &= y_0 + l_b s_{\phi_0} + l_1 s_{\phi_1}\\
x_2 &= x_0 + l_b c_{\phi_0} + l_1 c_{\phi_1} + l_1 c_{\phi_1} + l_2 c_{\phi_2}\\
y_2 &= y_0 + l_b s_{\phi_0} + l_1 s_{\phi_1} + l_1 s_{\phi_1} + l_2 s_{\phi_2}
\end{aligned} \quad (5)$$

The previous discussion shows that the system has five degrees of freedom (DoF). Different subsets out of the whole set of fourteen coordinates could be used according to the modeling approach followed. When modeling a manipulator in the EL context is a common practice to consider the relative angles between links as generalized coordinates, and the torques applied at the joints as generalized input forces. The corresponding choice of the vector q would then be $q_\theta = [x_0,y_0,\phi_0,\theta_1,\theta_2]$. As the EL model presented in this paper is derived from a BG, which considers inertial velocities, the angles ϕ_1,ϕ_2 measured with respect to the inertial frame will be used, instead of the relative angles θ_1,θ_2. To this choice corresponds the set $q=[x_0,y_0,\phi_0,\phi_1,\phi_2]^T$. No matter which set of independent generalized coordinates is used, the general form of a robot model derived from (1) is given in equation (6).

$$M(q)\,\ddot{q} + C(q,\dot{q})\,\dot{q} + R(q)\,\dot{q} + G(q) = W(q)\,T \quad (6)$$

Here $M(q)$ is the symmetric, positive definite inertia matrix, $C(q,\dot{q})$ is the Coriolis and Centrifugal matrix, $R(q)$ is the matrix of dissipative forces, $G(q)$ is the matrix of gravitational forces and $W(q)$ is a matrix that weights the input torques T. Notice that, for the robot under consideration, $R(q)$ and $G(q)$ are equal to zero since no friction and only planar movement on a horizontal base have been considered. Under these conditions, the model reduces to (7).

$$M(q)\ddot{q} + C(q,\dot{q})\dot{q} = W(q)\,T \quad (7)$$

The first BG presented, from now on called *the base BG* and denoted BG1, will be constructed relating its 1-junctions to the velocities associated to the dependent set $q_{BG1} = [\Omega_{w1},\Omega_{w2},\Omega_{w3},x_0,y_0,\phi_0,x_1,y_1,x_2,y_2,\phi_1,\phi_2]^T$. As it has 12 components, i.e., 7 more than the number of DoF, there are algebraic dependencies among their associated velocities, fact that will produce a BG with dependent storages, leading to what is called –in the jargon of the BG community – derivative causality or ZCP.

3. BG MODEL OF THE PLANAR ROBOTIC MANIPULATOR

The base BG is built following the standard procedure for mechanical systems briefly detailed below (Karnopp, Margolis and Rosenberg, 2006). It needs the relationships among the different velocities considered in the model, i.e., among the time derivatives of the components of vector q_{BG1}.

3.1. Construction of the base BG

Equation (8), expressing the relationships between the rotational velocities of the wheels, i.e. $\dot{\Omega}_w = \left[\dot{\Omega}_{w1},\dot{\Omega}_{w2},\dot{\Omega}_{w3}\right]^T$, and the velocities associated to the MB, i.e, $\dot{q}_{1-3} = \left[\dot{x}_0,\dot{y}_0,\dot{\phi}_0\right]^T$, can be obtained analyzing the geometry of the MB and the arrangement of the wheels. The shorthand notation $q_{1-3} := [x_0,y_0,\phi_0]^T$ has been used here. On the other hand, equation (9), obtained taking the time derivatives of (5), expresses the relationships between the Cartesian velocities of the CoM of the links, i.e. $\dot{z} := [\dot{x_1},\dot{y_1},\dot{x_2},\dot{y_2}]^T$, and the vector of velocities associated to the coordinates $q=[q_{1-3},\phi_1,\phi_2]^T$ of the MB-MA. $J_1(\phi_\mathrm{i})$ is the Jacobian associated to (5).

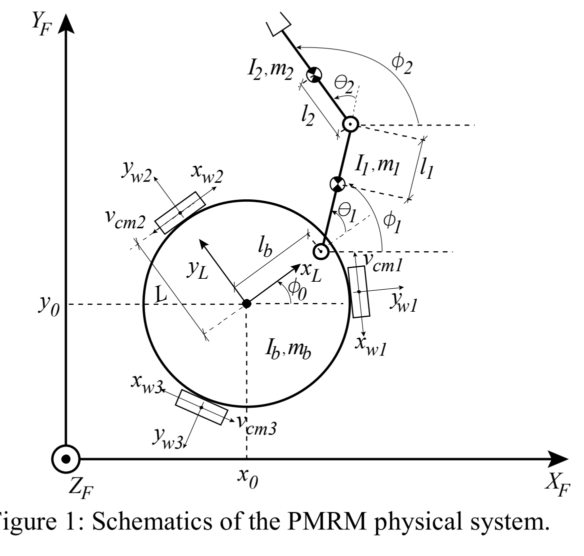

Figure 1: Schematics of the PMRM physical system.

$$\dot{\Omega}_w = \underbrace{\frac{1}{r}\begin{pmatrix} c_{\phi_0-\frac{\pi}{3}} & s_{\phi_0-\frac{\pi}{3}} & -L \\ c_{\phi_0} & s_{\phi_0} & -L \\ c_{\phi_0+\frac{\pi}{3}} & s_{\phi_0+\frac{\pi}{3}} & -L \end{pmatrix}}_{A_r(\phi_0)=\frac{1}{r}A(\phi_0)} \dot{q}_{1-3} \tag{8}$$

$$\dot{z} = \underbrace{\begin{pmatrix} 1 & 0 & -l_b s_{\phi_0} & -l_1 s_{\phi_1} & 0 \\ 0 & 1 & l_b c_{\phi_0} & l_1 c_{\phi_1} & 0 \\ 1 & 0 & -l_b s_{\phi_0} & -2l_1 s_{\phi_1} & -l_2 s_{\phi_2} \\ 0 & 1 & l_b c_{\phi_0} & 2l_1 c_{\phi_1} & l_2 c_{\phi_2} \end{pmatrix}}_{J_1(\phi_i)} \dot{q} \tag{9}$$

The BG interconnection structure is built using (8) and (9) by putting a 1-junction to represent each velocity, 0-junctions and MTFs to represent the sum of flows according to (9), and MTFs to represent the modulated power transfer among the different parts of the system. Finally the base BG, shown **in black color in** Figure 2, is completed by putting the I-elements (representing the storage of kinetic energy in the system) and the effort sources that model the torque inputs.

The causality assignment is carried out using the standard sequential causality assignment procedure (SCAP) (Karnopp, Margolis and Rosenberg, 2006). Integral causality can be assigned only to a proper subset of the I-elements of this BG, the choice being those attached to the 1-junctions associated with the $\dot{q}$ velocities. This restriction, as already anticipated due to the holonomic constraints (5) among the coordinates of the links, induces differential causality in some of the storage elements of the BG, with possible negative effects in numerical simulations of the model. To make it suitable for simulation tests, the BG of Figure 2 is adapted in the next subsection. For reasons of space and the sake of better understanding, the modifications –which consist in adding some elements and changing some causal strokes– are shown on the same Figure 2, with **the new elements represented in red color**.

3.2. BG for simulation purposes

Most current M&S software, particularly 20sim (Controllab Products, n.d.), a tool accepting model specification in the form of BG (among other usual formalisms), can deal with models featuring differential causality, i.e., in the presence of ZCPs. But not all M&S software applications are equipped with this tool, which is particularly necessary when the dependency among the storages is strongly nonlinear. This is the case of the BG1, where this dependency is given by the **MTF** structure having the matrices given in equations (8) and (9) as gains. Three different approaches helping to deal with ZCPs are treated next. The first one consists in breaking the ZCPs by adding effort residual sinks (**rSe**) elements. A residual sink is a computational device that injects the necessary effort (or flow) in order to make vanish the power conjugated variable entering into the sink, see the Appendix for a brief description. This element can be interpreted in the EL framework as the addition of Lagrange multipliers in the Lagrangian function. The second one breaks the causal loops by adding parasitic components between the statically coupled storages. As in this case these are I-elements, the pertinent parasitic components are C-elements, that must be of high stiffness in order to alter the dynamics the less possible. The third methodology eliminates the causal loops representing the whole energy storage by means of an *IC-Field* (Karnopp, 1992). Its equivalent is the use of a set of independent coordinates in the EL framework.

3.2.1. BG with rS to enforce integral causality

The addition of **rSe** done in red color in Figure 2 converts the implicit system of DAEs associated to the base BG into the explicit systems of DAEs, shown in (10), subject to restrictions (8) and (9).

$$\begin{aligned} M_1 \ddot{q} &= B(q)\,\lambda + W(q)\,T \\ M_2\,\ddot{z} &= C\,\lambda_{xy} \\ M_\Omega\,\ddot{\Omega}_w &= \tau_\Omega - \lambda_\Omega \end{aligned} \tag{10}$$

Where $M_1 = diag(m_b, m_b, I_b, I_1, I_2)$, $\lambda = [\lambda_\Omega, \lambda_{xy}]^T$, $\lambda_{xy} = [\lambda_{x1}, \lambda_{y1}, \lambda_{x2}, \lambda_{y2}]^T$, $\lambda_\Omega = [\lambda_{\Omega1}, \lambda_{\Omega3}, \lambda_{\Omega3}]^T$, $\tau_\Omega = [\tau_{\Omega1}, \tau_{\Omega2}, \tau_{\Omega3}]^T$, $T = [\tau_\Omega, \tau_1, \tau_2]^T$, $M_\Omega = diag(I_{w1}, I_{w2}, I_{w3})$, $M_2 = diag(m_1, m_1, m_2, m_2)$,

$$B(q) = \begin{bmatrix} A_r(\phi_0) & \begin{matrix} -1 & 0 & 0 & 0 \\ 0 & -1 & 0 & 0 \\ l_b S_{\phi_0} & -l_b C_{\phi_0} & 0 & 0 \end{matrix} \\ 0_{2X3} & \begin{matrix} l_1 S_{\phi_1} & -l_1 C_{\phi_1} & l_1 S_{\phi_1} & -l_1 C_{\phi_1} \\ 0 & 0 & l_2 S_{\phi_2} & -l_2 C_{\phi_2} \end{matrix} \end{bmatrix}$$

$$W(q) = \begin{bmatrix} A_r^{\,T}(\phi_0) & \begin{matrix} 0 & 0 \\ 0 & 0 \\ -1 & 0 \end{matrix} \\ 0_{2X3} & \begin{matrix} 1 & -1 \\ 0 & 1 \end{matrix} \end{bmatrix}, C = \begin{bmatrix} 1 & 0 & -1 & 0 \\ 0 & 1 & 0 & -1 \\ 0 & 0 & 1 & 0 \\ 0 & 0 & 0 & 1 \end{bmatrix}$$

The variables $\lambda_{x1,2}$, $\lambda_{y1,2}$ and $\lambda_{\Omega1,2,3}$ are the outputs of the residual sinks, see Figure 2.

Remark 1. It is stressed here that (10) is equivalent to the operations performed by the simulator solver processing the BG model, i.e., obtaining this equation system is not a task for the user of the M&S software.

Even with M&S software able to solve numerically the added constraints at each integration step, as 20Sim does for this example, it is in general convenient to solve the algebraic restrictions explicitly offline, and then to add them to the model, as this strongly reduces the computational cost of the simulation. This is done by taking the time derivative over (8) and (9) which results in (11)

$$\begin{aligned} \ddot{z} &= J_1(\phi_i)\ddot{q} + \dot{J}_1(\phi_i)\dot{q} \\ \ddot{\Omega}_w &= [A_r(\phi_0) \quad 0_{3x2}]\ddot{q} + [\dot{A}_r(\phi_0) \quad 0_{3x2}]\dot{q} \end{aligned} \tag{11}$$

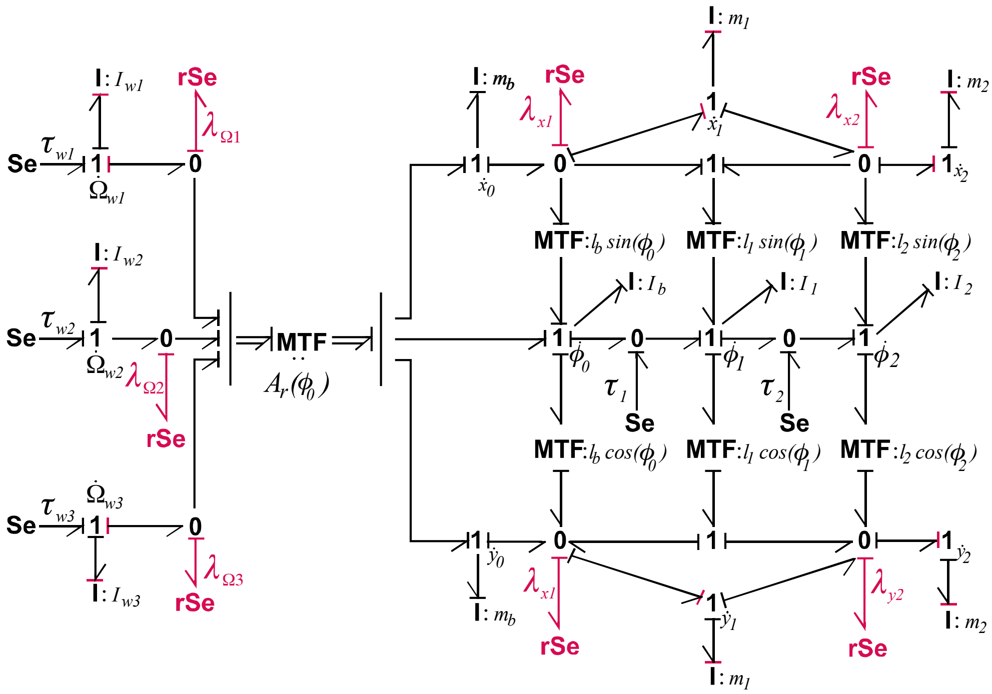

Figure 2: BG model of the planar robotic manipulator. **In black**: base BG with derivative causality. **In red**: residual sinks added to enforce integral causality in all the storage elements, and modified causal strokes for the originally dependent storages.

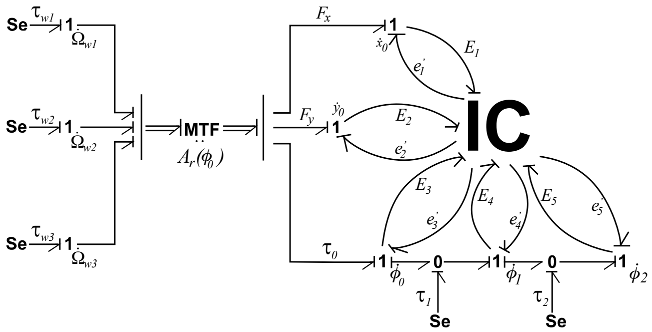

Figure 3: BG model using an *IC-Field*.

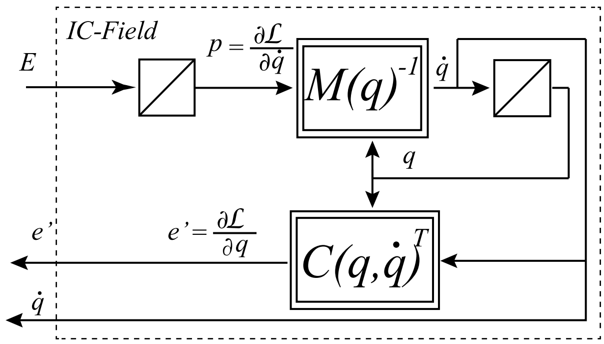

Figure 4: Block diagram of the *IC-Field*.

$$
M_{bl}(q)=\begin{pmatrix}
m_b+m_1+m_2 & 0 & -(m_1+m_2)l_bS_{\phi_0} & -(m_1+2m_2)l_1S_{\phi_1} & -m_2l_2S_{\phi_2}\\
0 & m_b+m_1+m_2 & (m_1+m_2)l_bC_{\phi_0} & (m_1+2m_2)l_1C_{\phi_1} & m_2l_2C_{\phi_2}\\
* & * & I_b+m_1l_b^2+m_2l_b^2 & (m_1+2m_2)l_1l_bC_{\phi_1-\phi_0} & m_2l_2l_bC_{\phi_2-\phi_0}\\
* & * & * & I_1+m_1l_1^2+4m_2l_1^2 & 2m_2l_1l_2C_{\phi_2-\phi_1}\\
* & * & * & * & I_2+m_2l_2^2
\end{pmatrix}
$$

$$
C_{bl}(q,\dot{q})=\begin{pmatrix}
0 & 0 & -(m_1+m_2)l_bC_{\phi_0}\dot{\phi}_0 & -(m_1+2m_2)l_1C_{\phi_1}\dot{\phi}_1 & -m_2l_2C_{\phi_2}\dot{\phi}_2\\
0 & 0 & -(m_1+m_2)l_bS_{\phi_0}\dot{\phi}_0 & -(m_1+2m_2)l_1S_{\phi_1}\dot{\phi}_1 & -m_2l_2S_{\phi_2}\dot{\phi}_2\\
0 & 0 & 0 & -(m_1+2m_2)l_1l_bS_{\phi_1-\phi_0}\dot{\phi}_1 & -m_2l_2l_bS_{\phi_2-\phi_0}\dot{\phi}_2\\
0 & 0 & (m_1+2m_2)l_1l_bS_{\phi_1-\phi_0}\dot{\phi}_0 & 0 & -2m_2l_1l_2S_{\phi_2-\phi_1}\dot{\phi}_2\\
0 & 0 & m_2l_2l_bS_{\phi_2-\phi_0}\dot{\phi}_0 & 2m_2l_1l_2S_{\phi_2-\phi_1}\dot{\phi}_1 & 0
\end{pmatrix} \tag{12}
$$

$$
\lambda=\left(\begin{bmatrix}M_\Omega & 0\\ 0 & M_2\end{bmatrix}\begin{bmatrix}A_r(\phi_0) & 0_{3x2}\\ & J_1(\phi_i)\end{bmatrix}M_1^{-1}B(q)-\begin{bmatrix}-I_{3x3} & 0_{3x4}\\ 0_{4x3} & C\end{bmatrix}\right)^{-1}
$$
$$
\left\{-\begin{bmatrix}M_\Omega & 0\\ 0 & M_2\end{bmatrix}\begin{bmatrix}A_r(\phi_0) & 0_{3x2}\\ & J_1(\phi_i)\end{bmatrix}M_1^{-1}W(q)\tau-\begin{bmatrix}M_\Omega & 0\\ 0 & M_2\end{bmatrix}\begin{bmatrix}\dot{A}_r(\phi_0) & 0_{3x2}\\ & \dot{J}_1(\phi_i)\end{bmatrix}\dot{q}+\begin{bmatrix}\tau_\omega\\ 0_{3x1}\end{bmatrix}\right\} \tag{13}
$$

Then, replacing (11) into the second and third equation of (10) results in (14).
Further, taking the first equation of (10) into (14) results in an explicit solution for λ as in (13). Then using (13) in (10) an explicit set of state equations is obtained.
Remark 2. It is stressed here that the BG-processor takes care of solving (10) (implicit in the BG) and (13), which must be first obtained by the user and then programmed in the BG in place of the rS.

$$\begin{bmatrix} M_\Omega & 0\\ 0 & M_2\end{bmatrix}\begin{bmatrix} A_r(\phi_0) & 0_{3x2}\\ & J_1(\phi_i)\end{bmatrix}\ddot{q} + \begin{bmatrix} M_\Omega & 0\\ 0 & M_2\end{bmatrix}\begin{bmatrix}\dot{A}_r(\phi_0) & 0_{3x2}\\ & \dot{J}_1(\phi_i)\end{bmatrix}\dot{q} = \begin{bmatrix}-I_{3x3} & 0_{3x4}\\ 0_{4x3} & C\end{bmatrix}\lambda + \begin{bmatrix}\tau_\Omega\\ 0_{3x1}\end{bmatrix} \tag{14}$$

3.2.2. BG with parasite components to enforce integral causality

The rS can be interpreted as the limit case of a storage element with its internal parameter tending to zero (Borutzky and Cellier, 1996). Thus, a non-ideal implementation of a rS would be reached assigning a very low value to this parameter. As it would cause a response with high frequency contents, the addition of a R component of convenient value is suggested to quickly damp the fast dynamics. Moreover, these parasite components, can model the elasticity and the friction between links occurring at the bushings.

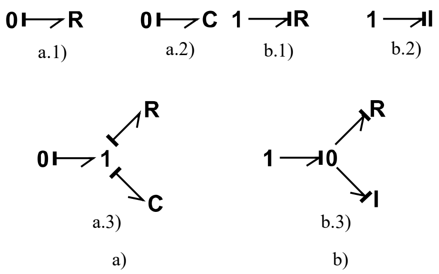

Figure 5: Residual sink replacing options for. a) **rSe**, b) **rSf**.

The use of parasite components to break algebraic loops is the most common solution among BG practitioners (Karnopp and Margolis, 1979) (Karnopp, Margolis and Rosenberg, 2006) as a method to eliminate derivative causality in multibody system models due to constraints introduced by mechanism joints, because its simplicity to achieve an explicit state equation set suitable for simulation without the need of extra calculations. As counterpart, the parametrization task of this extra component is usually difficult; moreover, this practice results in numerical stiff models. A parameter selection method based on the energetic activity of the parasitic components can be found in (Rideout and Stein, 2003) as well as an account of other techniques previously contributed within the bond graph community. Using this approach the BG model can be obtained replacing the rS components by the options depicted in Figure 5.

3.2.3. BG with storage IC-Field

The BG-theory recognizes explicit and implicit fields (Karnopp, Margolis and Rosenberg, 2006). The latter results when incorporating several (possibly single-port) components of akin type into a unique multiport device. This technique can be applied to BGs with derivative causality in order to eliminate it by subsuming the dependent storage elements with others in integral causality, building in this way one or more storage fields. Here all the energy stored in the system will be captured in a unique mixed-energy *IC-Field*. Even if there is no potential energy in the system, the C-part in the field appears because the topological coupling through the MTFs among the I-elements depends on the coordinates.
There are alternative ways of doing this, but all of them rely on the same rationale. It will be explained at an abstract level considering the EL model (7), taking into account that it can be extracted from the base BG of Figure 2, i.e, there is a direct correspondence between both descriptions. The details can be checked in (Karnopp, 1992). Equation (7) is a (vector) effort balance, which in a BG would occur at a (vector- or field-) 1-junction. The first term on the left-hand side would be the time derivative of the momentum-vector $p = \partial\mathcal{L}/\partial\dot{q}$ of an I-multiport attached to the 1-junction via a multibond, the second term would be the effort generated by a C-multiport attached to the same junction. Due to the dependence of both matrices M and C on q, both energy-storing fields constitute in fact a unique mixed *IC-field*. The second member of the equation is interpreted as the action of the (vector of) sources acting on the system through a $\boldsymbol{MTF}$ of matrix modulus $W(q)$ and the 1-junction. See the detailed expressions ofthe matrices $M(q)$ and $C(q, \dot{q})$ in equations (15), (16) and(12).
The resulting BG model is shown in Figure 3. Every vector component referred-to above, up to the *IC-Field*, is shown in its details, i.e., via its scalar components (the three 1-junctions on the left excluded, as they do not belong to the vector 1-junction; they are just shown to improve the understanding of the BG through the annotation of the wheels velocities). The constitutive relationships of the storage *IC-Field* defined in this way is depicted in the block diagram of Figure 4, where each integrator symbol stands for 5 scalar integration operations. This model solves the problems associated with differential causality assignment in the storage elements via the representation of the whole energy in a single storage field.

4. FROM BG MODELS TO EL AND PHS MODELS

In this section the method presented in (Karnopp, 1977) is employed to derive the EL model from the base BG. Then the PHS model is derived from the BG model with the storage *IC-Field*.

4.1. From BG to EL equations.

The procedure to obtain the EL equations of motions from a BG (Karnopp, 1977) is briefly detailed next:

1. Assign causality to all effort and flow sources (Se and Sf) and extend the causality through the structure of the model.

2. Choose a 1-Junction for which the flow has not been imposed and add an artificial flow source (Sf) to this junction.
3. Assign causality to the artificial flow source and extend it through the structure of the model.
4. Repeat the step 2 and 3 until all the bonds have been causally oriented.
5. Label the flows imposed by the artificial flow sources as $\dot{q}_i$.
6. Using the standard equation-reading procedure based on the causality assignment, read the incoming efforts to the artificial flow sources and express them in terms of the $\dot{q}_i$.

Placing the *artificial flow sources* at the 1-junctions associated with the vector $\dot{q} = [\dot{x}_0, \dot{y}_0, \dot{\phi}_0, \dot{\phi}_1, \dot{\phi}_2]^T$, i.e. *choosing* the outputs of the storage elements in integral causality in the BG of Figure 2 as generalized velocities $\dot{q}_i$, would yield $q = [x_0, y_0, \phi_0, \phi_1, \phi_2]^T$ as *the vector of generalized coordinates*. Because of space restrictions the procedure just described is not shown graphically here, but it is stressed that following it the EL equations derived from the base BG of Figure 2 are the same given in (7), with the following particular expressions for the matrices $M(q)$ and $C(q, \dot{q})$ (detailed expressions for $M_{bl}(q)$ and $C_{bl}(q, \dot{q})$ are given in (12)):

$$M(q) = M_{bl}(q) + \begin{bmatrix} A^T(\phi_0)M_{\Omega}A(\phi_0) & 0_{3X2} \\ 0_{2X3} & 0_{2X2} \end{bmatrix} \quad (15)$$

$$C(q, \dot{q}) = C_{bl}(q, \dot{q}) + \begin{bmatrix} A^T(\phi_0)M_{\Omega}\dot{A}(\phi_0) & 0_{3X2} \\ 0_{2X3} & 0_{2X2} \end{bmatrix} \quad (16)$$

4.2. From BG to PHS models.

The method presented in (Donaire and Junco, 2009) to obtain a PHS from the BG model of Figure 2 cannot be applied directly since the causal path that relates the storage elements in derivative and integral causality pass through a **MTF** which depends on the state variables. However, see (Donaire and Junco, 2009) for a detailed definition, the relationship between the BG and the PHS variables are the same, i.e. the inputs and outputs of the storage elements in integral causality are, respectively, the time derivatives $\dot{p}$ and $\dot{q}$ of the state vectors and the components of the gradient of $\mathcal{H}(p, q)$.
Here an explicit PHS is obtained from the BG of Figure 3 considering the *IC-Field* model of Figure 4. Reading through the causal paths on Figure 3, the relationship between the state vector and the gradient components can be obtained. From these relationships the skew symmetric structure matrix is computed. Then, reading through the causal paths from the sources to the *IC-Field*, the matrix that weights the inputs is obtained. Altogether this results in the PHS expressed in (17).

$$\begin{pmatrix} \dot{q} \\ \dot{p} \end{pmatrix} = \begin{pmatrix} 0 & \mathrm{I}_{5x5} \\ -\mathrm{I}_{5x5} & 0 \end{pmatrix} \nabla_x \mathcal{H} + \begin{pmatrix} 0 \\ W(q) \end{pmatrix} T \quad (17)$$

5. SIMULATIONS RESULTS

All the models derived from the base BG model are well-suited for simulation and control system design (at least to tune the control law via simulation experiments), but not all of them are good for model-based controller synthesis. Here, the distinction between control system synthesis, referring to the derivation of the control law, and control system design, denoting its parameterization, has been made, following Wonham (Wonham, 1979). It is not the purpose of this paper to provide new control laws nor a new method to obtain them, but just to point out the suitability of the previous models to these aims. Tuning controllers with the help of simulation is a typical method used, for instance, to adjust the gains of a PD controller taking care of point-to-point missions. On the other hand, only the BG with the IC-field and, of course, the EL and PHS models, are suitable for control system synthesis, as this needs a proper system model. Indeed, the BG with the residual sink is not, as it shows all the energy variables in integral causality, thus having an artificially created excess of state variables. Nor is suitable for this purpose the BG with the parasitic spring-damper components, because it contains the spurious states associated to the spring energy variables. Readers interested in methods for control system synthesis and design of robotic manipulators affine to the modeling techniques considered in this paper, could refer to (Siciliano et al., 2009) and (Ortega et al., 2013) for classic and energy-based methods, and to (Merzouki et al., 2012) for methods in the BG-domain.
The model parameters of the links are: $m_1 = 0.5Kg$, $l_1 = 0.5m$, $I_1 = 0.0015Kgm^2$, $m_2 = 0.5Kg$, $l_2 = 0.25m$, $I_2 = 0.0012Kgm^2$. The simulation parameters of the MB are: $I_{w1} = 0.1\ Kgm^2$, $I_{w2} = 0.1Kgm^2$, $I_{w3} = 0.1Kgm^2$, $r = 0.05m$, $l_b = 0.15m$ and $L = 0.2m$.
All the models were simulated in 20sim® (Controllab Products, n.d.), in closed loop with the same control law, a feedback-linearization based tracking controller, see (Siciliano et al., 2009) for a detailed description of the control scheme (resulting from an EL-model based design). The Modified Backward Differentiation Formula (MDF) has been selected as the integration method, with a tolerance for relative and absolute errors of 1e-5.
In this section two simulation scenarios are addressed. In the first scenario the desired end effector trajectory is a circumference of radius $R = l_1 + l_2$ with center at the origin of link 1. As the PMRM is redundant, infinite configurations of vector q can realize the desired trajectory. In this particular scenario, the end effector trajectory is achieved by moving only link 1 while the other coordinates remain constant. The performance of the model is analyzed taking into account the simulation time and the integral of the error e defined in (18), where (x, y) and (x_{ref}, y_{ref}) are the end effector position and desired end effector position respectively.

$$e = \sqrt{\left(x - x_{ref}\right)^2 + \left(y - y_{ref}\right)^2} \quad (18)$$

All the four BGs previously presented have been simulated in this scenario. Table 1 presents the results. The three first simulations present a similar behavior regarding the errors. Even though their values are quite similar, the simulation time of the BG model with derivative causality is higher. This behavior suggests that the numerical solution of BG with derivative causalities takes less time if ZCPs are broken adding residual sink efforts or parasitic components. However, in the latter case, as parasitic components are a non-ideal implementation of residual sinks, there will be a dependency of the simulation errors on the parameter tuning criteria. Finally, as it can be seen, the *IC-Field* method presents the smallest error, a consequence of the exact cancellation by the controller of nonlinearities in the *IC-Field* BG. But this advantage has a negative counterpart: implementing the *IC-Field* implies inverting the system inertia matrix in the BG model (precisely the nonlinearity cancelled by the controller), the cause of the increase in simulation time with respect to the two previous models. In this simple system this increase is not an issue, but may noticeably slow down the simulation in more complex systems.

Table 1: Simulation times and errors.

BG Simulations models	Simulation Time [s]	Error
BG with derivative causality	2.302	0.1838
BG with rS (*constraint*)	0.495	0.1839
BG with parasitic components	0.453	0.1861
BG with *IC-Field*	0.732	0.0021

The evolution of the positions in the simulation of the *IC-Field* model are shown in Figure 6. Starting from the initial condition $q_0 = [4.35,0,0,0,0]^T$ and zero velocities, the circular trajectory is followed. Figure 7 depicts the error (18).

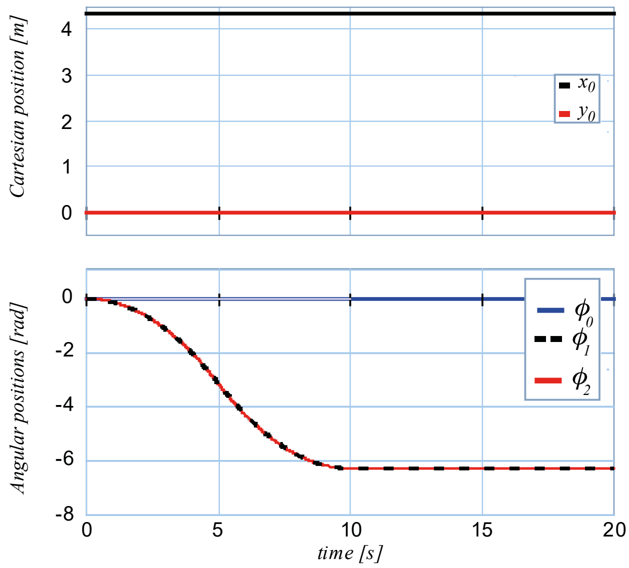

Figure 6: Evolution of the positions in the BG with *IC-Field*.

The second scenario has two stages: in the first, the MB moves from the initial condition $q_0 = [0,0,0,0,0]^T$ to the point $q = [4.35,0,0,0,0]^T$. In the second, once that point reached, the end effector describes a circumference of radio $R = l_1 + l_2$ by moving only link 1. The evolutions of all the generalized positions are depicted in Figure 8. Figure 9 shows the trajectory performed by both the end effector and the tip of link 1 for this scenario.

It is concluded that all the BG models are useful for the numerical test of the closed-loop performance.

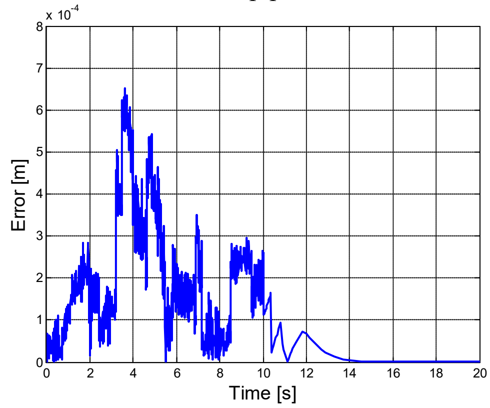

Figure 7: Evolution of the error in the *IC-Field* BG model.

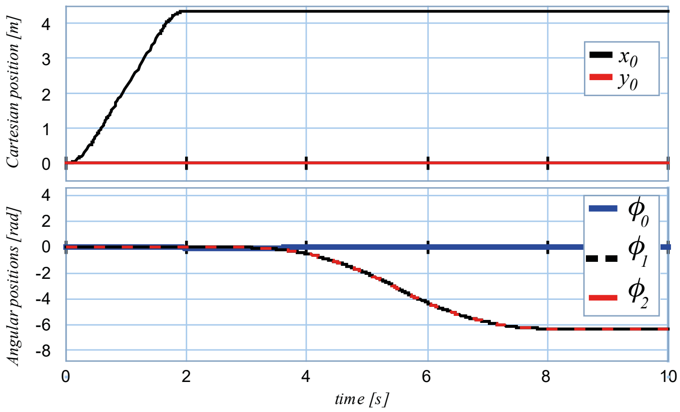

Figure 8: Evolution of the generalized positions in the BG with *IC-Field* in scenario 2.

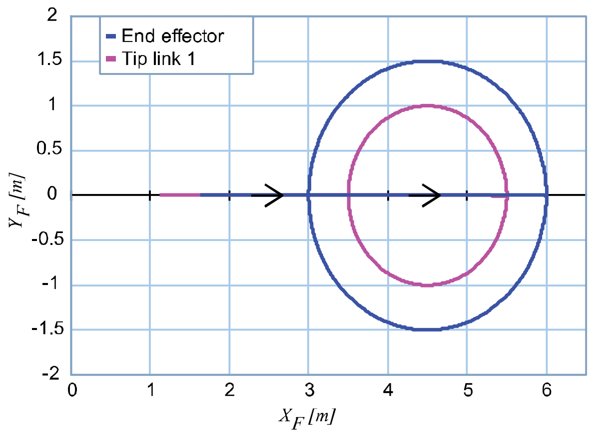

Figure 9: End efector and tip of link 1 in workspace.

6. CONCLUSIONS

In this paper a BG model of a planar mobile robotic manipulator was obtained with the standard BG-modeling procedure. This model presents nonlinear state-dependencies among storage elements that could be inconvenient for, or not manageable by numerical solvers of some simulation tools. As solutions to this problem, three modifications of the base BG model have been presented. These modifications consist in breaking the ZCP by adding parasitic elements or, alternatively, rS, and introducing storage fields with energy variables without constraints. Also, the inherent properties of BGs have been exploited to derive from the base BG Euler-Lagrange and Port-Hamiltonian models, the two main energy-based modeling formalisms used for control system design. Even though the main objective of this work was not the design of the controller for the planar mobile robotic manipulator, a model based control technique has been implemented in order to perform simulation allowing to validate the BG models.

ACKNOWLEDGMENTS
The authors wish to thank SeCyT-UNR for the support to this research through the financing of PID-UNR_ING502, and MinCyT (Argentina) and DST (India) for the financing of project IN/14/07 in the framework of the bilateral cooperation between Argentina and India.

APPENDIX: RESIDUAL SINKS
A residual sink element, graphically represented in Figure 10, can be interpreted as an energy-storing device whose parameter tends to zero. For example, an effort residual sink can be interpreted a C element in integral causality:

$$C\dot{e} = \Delta f \tag{19}$$

If the parameter C tends to zero, then $\dot{e}$ is determined by the algebraic equation $\Delta f = 0$.

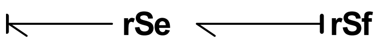

Figure 10: Effort and flow residual sinks.

REFERENCES

Borutzky, W. and Cellier, F.E. (1996) 'Tearing Algebraic Loops in Bond Graphs', *Trans. Soc. Comput. Simul. Int.*, vol. 13, #dec#, pp. 102-115, Available: ISSN: 0740-6797.

Cacho, R., Felez, J. and Vera, C. (2000) 'Deriving simulation models from bond graphs with algebraic loops.', *Journal of the Franklin Institute*, vol. 337, pp. 579-600, Available: ISSN: 0016-0032.

Controllab Products, B.V. (n.d) *20-sim. www.20sim.com*, Available: http://www.20sim.com.

Donaire, A. and Junco, S. (2009) 'Derivation of Input-State-Output Port-Hamiltonian Systems from bond graphs', *Simulation Modelling Practice and Theory*, vol. 17, pp. 137-151, Available: ISSN: 1569-190X.

Gawthrop, P.J. and Smith, L. (1992) 'Causal augmentation of bond graphs with algebraic loops', *Journal of the Franklin Institute*, vol. 329, pp. 291-303, Available: ISSN: 0016-0032.

Karnopp, D. (1977) 'Lagrange's Equations for Complex Bond Graph Systems.', *ASME. J. Dyn. Sys., Meas., Control.*, vol. 99, pp. 300-306.

Karnopp, D. (1992) 'An approach to derivative causality in bond graph models of mechanical systems', *Journal of the Franklin Institute*, vol. 329, pp. 65-75, Available: ISSN: 0016-0032.

Karnopp, D. and Margolis, D. (1979) 'Analysis and Simulation of Planar Mechanism Systems Using Bond Graphs',. *ASME. J. Mech. Des.*, vol. 101, pp. 187-191.

Karnopp, D., Margolis, D. and Rosenberg, R. (2006) *System Dynamics: Modeling and Simulation of Mechatronic Systems*, New York, NY, USA: John Wiley & Sons, Inc.

Merzouki, R., Samantaray, A.K., Pathak, P.M. and Bouamama, B.O. (2012) *Intelligent Mechatronic Systems: Modeling, Control and Diagnosis*, Springer Publishing Company, Incorporated.

Nacusse, M.A. and Junco, S.J. (2017) 'Controlled Switched Structures for Bond-Graph Modelling and Simulation of Hybrid Systems', in Borutzky, W. (ed.) *Bond Graphs for Modelling, Control and Fault Diagnosis of Engineering Systems*, Cham: Springer International Publishing.

Ortega, R., Perez, J.L., Nicklasson, P. and Sira-Ramirez, H. (2013) *Passivity-based control of Euler-Lagrange systems: mechanical, electrical and electromechanical applications*, Springer Science \& Business Media.

Ortega, R., Schaft, A.J.V.D., Mareels, I. and Maschke, B. (2001) 'Putting energy back in control', *IEEE Control Systems*, vol. 21, Apr, pp. 18-33, Available: ISSN: 1066-033X.

Ortega, R., Spong, M.W., Gomez-Estern, F. and Blankenstein, G. (2002) 'Stabilization of a class of underactuated mechanical systems via interconnection and damping assignment', *IEEE Transactions on Automatic Control*, vol. 47, no. 8, Aug, pp. 1218-1233, Available: ISSN: 0018-9286 DOI: 10.1109/TAC.2002.800770.

Rideout, G. and Stein, J.L. (2003) 'An Energy-Based Approach to Parameterizing Parasitic Elements for Eliminating Derivative Causality', Proc. ICBGM'03, the Int. Conf. on Bond Graph Modeling and Simulation, Orlando, 121–128.

Siciliano, B., Sciavicco, L., Villani, L. and Oriolo, G. (2009) *Robotics: Modelling, Planning and Control*, Springer.

van der Schaft, A. and Jeltsema, D. (2014) 'Port-Hamiltonian Systems Theory: An Introductory Overview', *Found. Trends Syst. Control*, vol. 1, #jun#, pp. 173-378, Available: ISSN: 2325-6818.

van Dijk, J. and Breedveld, P.C. (1991) 'Simulation of system models containing zero-order causal paths—I. Classification of zero-order causal paths', *Journal of the Franklin Institute*, vol. 328, pp. 959-979, Available: ISSN: 0016-0032.

van Dijk, J. and Breedveld, P.C. (1991) 'Simulation of system models containing zero-order causal paths—II Numerical implications of class 1 zero-order causal paths', *Journal of the Franklin Institute*, vol. 328, pp. 981-1004, Available: ISSN: 0016-0032.

Wonham, W.M. (1979) *Linear Multivariable Control: A Geometric Approach*, 2nd edition, Springer-Verlag.